Controllable and Reversible Hot Spot Formation on Silver Nanorod Arrays

Justin L. Abell,[a†]* Jeremy D. Driskell,[b] and Yiping Zhao[a]

[a]Nanoscale Engineering and Science Center, University of Georgia, Athens, GA 30602
[b]Department of Chemistry, Illinois State University, Normal, IL 61790.

Supporting Information

S.1 Materials and Methods

AgNR SERS Substrate Fabrication

AgNR substrates were fabricated as described previously.[1, 2] Glass microscope slides were cut into appropriately sized pieces and then cleaned with piranha solution (H_2SO_4:H_2O_2, 4:1). After thoroughly rinsing with DI water and blow-drying with N_2, the glass substrates were loaded into a custom e-beam evaporator. The substrates were attached to a rectangular 5 in × 6 in stainless steel plate using double-sided tape. The glass pieces were arranged in precisely predefined positions so as to allow careful analysis of the location-dependent nanorod deposition. The chamber was pumped to a pressure of at least 10^{-6} Torr before starting the deposition. The deposition thickness and rate was monitored with a quartz crystal microbalance (QCM) directly facing the source material. A variable shutter was used to allow fabrication of different length AgNRs onto substrates located at different positions on the metal plate.

Two types of substrates were prepared: One group of AgNR substrates was fabricated without an underlying Ag film. For these substrates, the substrate normal was initially positioned at $\theta = 86^{o}$ with respect to the incident vapor direction. Ti (Kurt J. Lesker, 99.995%)

was used as an adhesive layer and evaporated at a rate of 1.0-3.0 Å/s until a final QCM thickness of 20 nm. Then Ag (Kurt J. Lesker, 99.999%) was evaporated at 2.0-4.0 Å/s until a final QCM thickness reading of 2000 ± 20 nm was achieved. For the second group of substrates, the same deposition conditions were used except that the Ti film was first deposited with the substrate normal parallel to the incident vapor direction (i.e $\theta = 0^{o}$), which yielded a thin film rather than OAD structures. Next Ag was deposited at the same angle until a QCM thickness of 200 nm was achieved. After the Ag thin film was deposited, the substrate holder was rotated 86^{o} and the Ag deposition was continued for another 2000 ± 20 nm as reported by the QCM. After the desired AgNR film thickness was achieved, the deposition was stopped and the substrates were allowed to cool in vacuum before removing from the chamber.

SERS Instrumentation and Spectral Analysis

All Raman and SERS measurements were acquired using an Enwave 10HT-HRC portable Raman system equipped with a 785 nm solid state laser coupled to probe tip via an optical fiber. All measurements were acquired at 30 to 180 mW, with integration time ranging from 1-90 seconds. The manufacturer states the focused beam spot diameter ≈ 100 µm. Most SERS measurements were performed by continuously rastering the laser spot across the AgNR film during the measurement acquisition so as to minimized excitation-induced changes in the spectra and also to sample a larger area of the AgNR film to a achieve a more representative SERS signal. Spectral peak fitting was performed using GRAMS/AI and OriginPro 9.0; all peaks were fit as convolutions of Gaussian and/or Lorentzian distributions.

Thiol Immobilization and In Situ SERS Analysis

Small 0.9 × 0.9 cm^2 AgNR substrates were used for all SERS analysis in this study. All sample solutions were prepared in Millipore 18 MΩ·cm water unless otherwise stated. Prior to thiol immobilization, AgNR substrates were pre-cleaned in a custom made inductively coupled Ar^+ plasma chamber when deemed necessary. The Ar pressure was 600-700 mTorr, the applied power was 30 W, and the substrates were exposed to the Ar^+ plasma for ~90 seconds.

For the mercaptophenol (MPh) vapor deposition onto AgNRs, a glass bowl was used that contained a reservoir of high concentration MPh solution (100 mM in isopropanol). AgNRs were placed onto an elevated stage in the middle of the bowl to keep the substrates dry. The bowl was covered and the AgNRs were allowed to incubate in the MPh vapor for approximately 20 minutes.

Other substrates were immersed into 1-4 mL of a liquid thiol solution at pre-defined concentrations in cleaned glass test tubes or glass petri dishes, allowing the AgNR substrate to be completely immersed in the sample solution during incubation. After incubating the AgNRs in the solution for a predetermined amount of time, the substrates were removed from the thiol solution and immediately rinsed thoroughly with deionized (DI) water before blow-drying with an inert gas such as N_2 or Ar. For measurements performed in liquid, the AgNRs substrates were placed into 4 mL of solvent in a small glass dish allowing SERS measurements to be acquired through the transparent solvent layer.

S.2 SERS Analysis of Vapor-Deposited MPh

The results of the MPh vapor-deposition confirm that the capillary action of a drying liquid film causes the AgNRs to bundle together, and that such a process is responsible for

producing the characteristically large signal intensity observed with AgNR SERS substrates. We also note that the AgNRs typically do not produce any significant signal from additional analytes added to the AgNRs after the first analyte has been added and the AgNRs dried/bundled (data not shown), i.e. additional analytes are occluded from the hot spots formed between the nanorod contact points. This observation too is also similar to that obtained by Schmidt et al.[3] After the initial MPh vapor deposition, we note that the AgNRs occasionally demonstrate an increase in intensity upon the initial immersion in the water (as opposed to the ~50% decrease typically observed), which could be due to bundling induced by the capillary forces of the solvent front during the initial immersion. Additionally, the AgNRs treated with MPh-vapor deposition occasionally demonstrated only ~ 2-fold increase in signal intensity after wetting and drying. Clearly, the quantitative reproducibility of the bundling experiments with the vapor-deposited MPh leaves much to be desired. This could be in part a result of the poor reproducibility of the surface coverage produced by vapor deposition of MPh on AgNR films. Considering that MPh has a highly hydrophilic –OH head group, variations in the MPh surface coverage on the AgNR surface could affect how strongly the water interacts with the surface. This would in turn affect the degree to which capillary forces are imparted on AgNRs during the wetting and drying process. Regardless, these experiments show that a large SERS signal enhancement is achieved after the AgNR film is wetted and subsequently dried.

S.3 SEM Analysis of Vertical Bundling of the AgNR film

Previous studies have demonstrated the effect of liquids on high aspect ratio nanostructures;[3-8] likewise, one may also anticipate OAD-generated AgNRs be mechanically susceptible to the forces imparted by a liquid's surface tension. We therefore performed an SEM

analysis of the AgNRs, with the aim of finding any structural changes induced after liquid treatment.

Scanning electron microscope images of the AgNR substrates were acquired using an FEI Inspect F FEG SEM. Cross-sectional SEM images of the AgNR substrates was acquired by splitting the AgNR substrate along the AgNR tilt direction after the AgNR films were fabricated.

AgNR film substrates were analyzed as-deposited, while the other substrates were first immersed in DI water and then dried before analysis. The SEM analysis was performed on two groups of substrates, with one group being placed at the bottom of the substrate holder during OAD (i.e. closest to the source material), while the other was at the top of the substrate holder (i.e. ~5 inches further away from the source material). A top view SEM analysis demonstrated no apparent difference in the nanorod tilting direction or uniformity for the two substrates (Figures S1A-B). The cross sectional morphology of the two substrates appeared similar at a cursory glance, but closer inspection showed that the AgNR film treated with water was approximately 10% thinner (Figures S1C-D). Because the observed differences between the two treatments are minor and to avoid subjective bias, a more rigorous and objective statistical analysis was performed. For each of the four substrates, five high-magnification cross-sectional images were acquired. For each image, the tilting angle ϕ of n = 10 OAD nanostructures was determined, and the film thickness T was estimated from each image. Thus, for each substrate n = 50 angles and n = 5 AgNR film thicknesses were measured.

From Figure S2 we can first see that the as-deposited AgNR films closer to the Ag source material during deposition demonstrate a thicker film than those at the top of the holder, yet both groups have essentially the same tilting angle ϕ as expected. For the thicker AgNR film, after the water-treatment T appears to change from 817 ± 52 nm to 748 ± 35 nm and the tilting angle

decreases from 15.1 ± 3.6 to 12.5 ± 4.4. For the thinner AgNR film, a similar trend is observed as the thickness decreases from 574 ± 33 nm to 546 ± 52 nm, and ϕ decreases from 14.4 ± 3.9 to 12.3 ± 4.9 degrees after water treatment. In both cases we see evidence for the expected decrease in AgNR film thickness, decrease in average ϕ, and increase in the disorder (i.e. standard deviation) of ϕ. Clearly, however, these changes are subtle, and based on the error bars from Figure S2, there is significant statistical overlap between the as-deposited and water-treated samples. Thus, in order to determine if ΔT and $\Delta\phi$ are statistically significant, we performed a paired Student's T-test. Accordingly, no statistical significance is observed before and after water treatment for T; however, the difference in ϕ between the as-deposited and the water-treated samples is indeed statistically significant for both groups. The fact that T does not yield a statistically significant difference could be a result of the relative few measurements used in the analysis (only n = 5 thickness measurements per substrate) and also the difficulty in visually determining precisely where the underlying Ag film ends and the AgNRs begin.

In conclusion, these findings are very similar to those reported by Fan et al. for OAD-generated SiNR[6]: although the SiNR morphology appeared to remain unchanged from a top view image, the results of solvent-induced bundling could be readily discerned without cross sectional SEM analysis. In that study the SiNR film became much more compact as ϕ and consequently T decreased. In addition, the untreated SiNRs demonstrated an extremely uniform tilting angle, but after treatment with water, significantly more disorder of the tilting angle was observed.[6] Thus, the SEM analysis appears to confirm the AgNR bundling phenomenon, but further investigation is warranted.

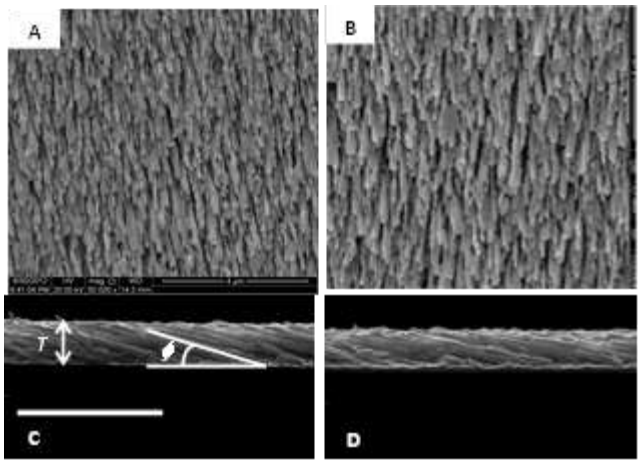

Figure S1. Overhead and cross sectional SEM images of AgNR film as-deposited (A and C) and after treatment with water (B and D). Both A and B have the same magnification; for C and D the scale bar is 3 μm. These substrates were from the bottom of the sample holder in the evaporation chamber.

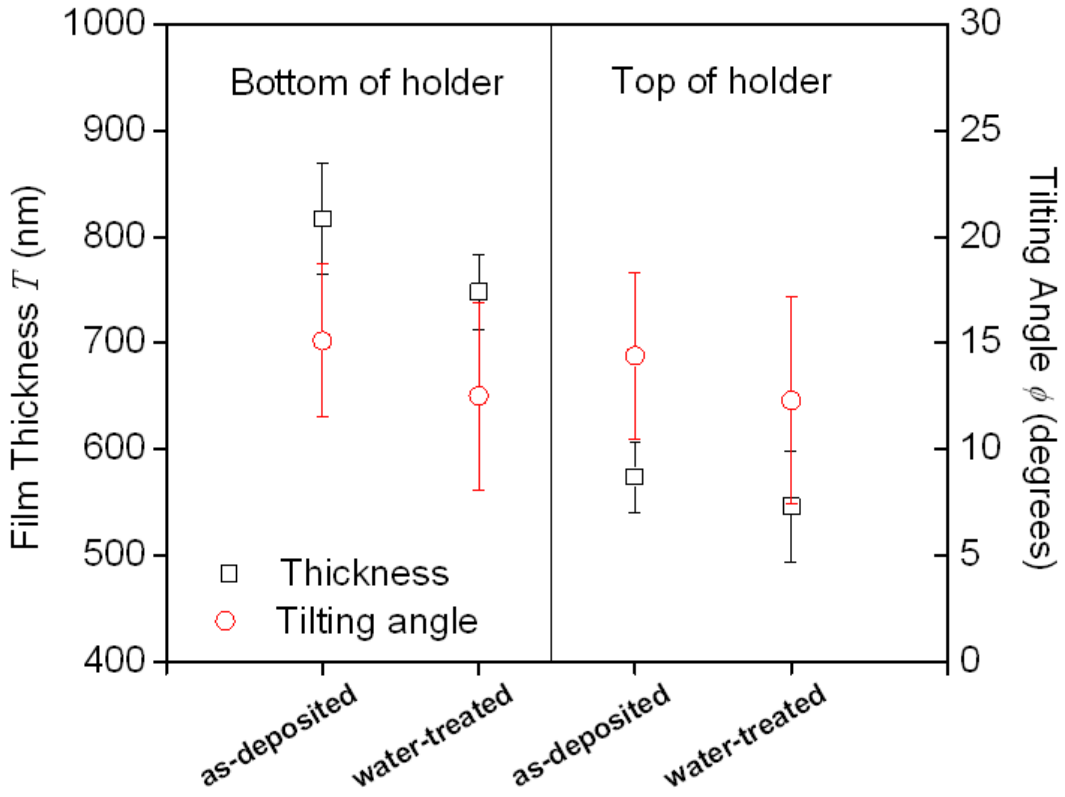

Figure S2. AgNR film thickness T and tilting angle ϕ statistics acquired from SEM images for two groups of substrates (bottom and top of sample holder) for as-deposited and water-treated.

S.4 Conductance Measurements of Solvent-Treated AgNR Films

One possible way to further confirm the nanobundling effect is to use sheet conductance measurements with a four point probe. Because the bundling phenomenon would possibily result in a more compact AgNR film (due to vertical bundling), with more direct contact between neighboring nanorods, the AgNR film could yield a significantly higher conductance.

A custom made four-pin/point probe was used to apply current to the AgNR film via the

outer pins while measuring the voltage across the two inner pins. Each pin has individual spring-loaded holder to assure the pin makes complete contact with the sample; the pins also have sharp tips so as to prevent significant damage to the AgNR film during contact. The pin-to-pin separation was 2.3 mm. The current was applied via a source meter that was interfaced with a custom LabVIEW program. The initial current was 1 mA and incrementally increased by 1 mA/step until a final current of 20 mA and the voltage was recorded at each interval. The resistance was calculated from the slope of the voltage vs. current measurements.

Conductance measurements were acquired on 1.8 x 1.8 cm^2 AgNR substrates fabricated without an underlying Ag film. For all measurements, the four pins were aligned approximately with the AgNR growth direction (i.e. measuring the conductance along the nanorod growth/tilt direction), and the four pins were placed in the center of the substrate to avoid potential edge effects. First, the conductivity was measured on as-deposited AgNRs. Afterwards, the substrate is briefly immersed into a liquid solvent and then immediately blow-dried with Ar.

Because the AgNRs are assumed to be rigid, an increase in sheet conductance must therefore be due to vertical bundling resulting from a decrease in the ϕ caused by bending where the nanorod connects to the underlying substrate. This implies that after bundling, a nanorod is primarily making contact with the nanorods directly in front of and behind it, and that these contact points will form conductive paths that instill the film with high sheet conductance in the direction of the nanorod tilt.

To test this, AgNR films were deposited to a QCM thickness of 2000 nm onto glass without the use of a continuous underlying Ag thin film. Prior to wetting, the sheet conductance of AgNR films on glass was low and in many cases yielded infinite resistance. If capillary-induced bundling produces a more compact film, more inter-rod contact points (and therefore

more hot spots) are likely to form; hence the conductance of the AgNR film is anticipated to increase. Because the solvent's surface tension γ is directly responsible for the bundling effect, one may expect that a change in γ could change the extent of AgNR bundling. Water has an exceptionally high surface tension of γ = 72.80 mN/m, and we may therefore expect it to yield a high AgNR film conductance. For comparison, isopropanol (IPA), toluene, hexane were also used because they have varying surface tensions (23.00, 28.40, 18.43 mN/m, respectively). These other solvents, with smaller γ, may be expected to exert less of a capillary force on the AgNRs during the drying process, ultimately yielding less AgNR bundling and therefore lower sheet conductance.

The results of this experiment are shown in Figure S3. After the water dries, the AgNRs yield a relatively high conductance of σ = 0.385 S. Hexane, with the lowest γ tested, yields a AgNR film conductance of σ = 0.117 S. Toluene only demonstrates a slightly higher conductance of σ = 0.122 S. IPA yielded a higher conductance of σ = 0.181 S, higher than that of toluene. To make sure this value was real and not an anomaly, a second AgNR substrate was treated with IPA which yielded σ = 0.259 S, which is somewhat higher than the first IPA-treatment conductance measurement, but still lower than water. The water treatment was also replicated on another substrate where σ = 0.392 S, which is nearly identical to that of the first water-treated film.

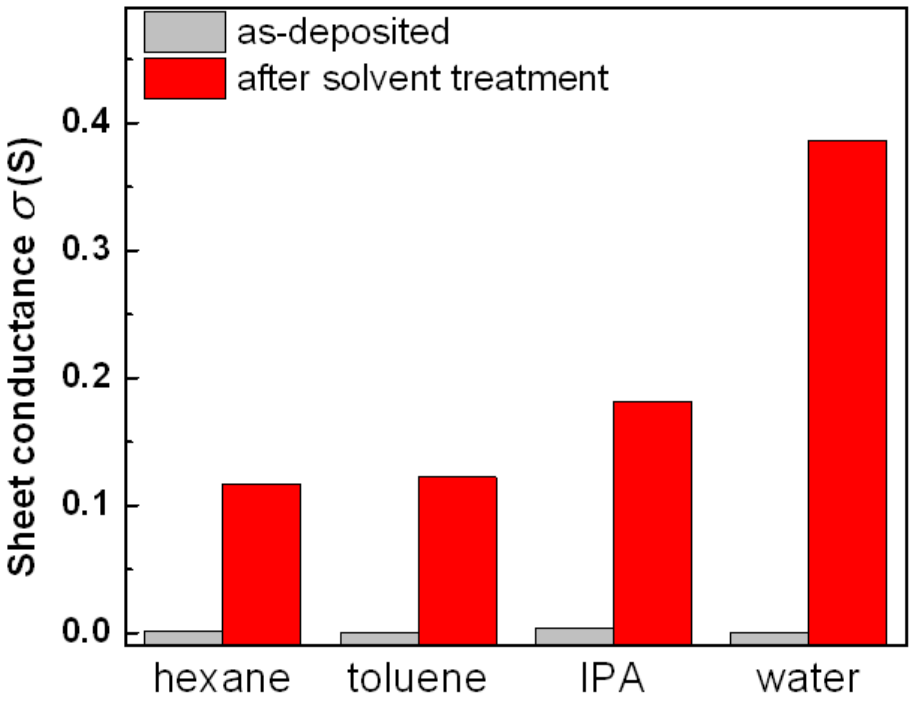

Figure S3. Sheet conductance σ of as-deposited AgNR films and after treatment with different solvents.

We point out that IPA has a surface tension in between that of hexane and toluene, but produces a significantly higher sheet conductance than toluene. The exact reason for this behavior is unclear, but could be a result of the interfacial surface energy of the solvents. This energy represents how strongly the solvent interacts with the Ag surface. Although IPA has a lower surface tension, it may interact more strongly with the AgNR surface, and therefore ultimately exert more capillary force on the AgNRs during the drying process. However, a detailed quantitative investigation of this behavior is beyond the scope of this study. Regardless of the particular solvent, after the AgNRs have been wetted and dried we find a drastic increase in the sheet conductance of the AgNR films tested in this experiment.

S.5 Bundling/SERS Effect for Variable Length AgNRs

One easy way to test this is to monitor how I_{wet}/I_{dry} changes as a function of nanorod length for AgNR films pre-treated with a monolayer of MPh. AgNR length is dependent on the deposition thickness *d*, which could be varied by using a variable shutter to expose different regions of the substrate holder to different *d* (measured by the QCM). Figure S4 shows the top and cross sectional views of the SEM images for d = 100, 150, 250, 350, and 500 nm. In addition, these AgNRs were deposited onto a 200 nm thick Ag film pre-deposited onto glass or Si pieces.

These AgNR films were first functionalized with a MPh monolayer as discussed previously, and then rinsed and I_{wet} measured, and then dried and I_{dried} was measured and then normalized to excitation power and integration time. The resulting I_{wet}/I_{dry} ratio function of the QCM thickness is shown in Figure S5. The AgNR films deposited with QCM = 50 and 100 nm, the AgNRs did not produce a sufficient SERS signal. Even at stringent measurement conditions (i.e. 180 mW and 60s excitation), these substrates failed to produce a detectable MPh peak at 1078 cm^{-1}, and but did produce a large peak at ~500 cm^{-1}, and smaller peaks at ~420 cm^{-1} and ~390 cm^{-1}, the latter possibly resulting from MPh. Regardless, we did not include these substrates in the analysis proceeding due to the ambiguity of the signal. From Figure S5 there is a clear dependence of *d* and the I_{wet}/I_{dry} ratio, i.e. as the nanorods become longer, I_{wet}/I_{dry} decreases from 0.78 to 0.06 between QCM thicknesses of 150 and 500 nm, respectively. As the nanorods grow longer (QCM = 1200 nm), the I_{wet}/I_{dry} increases slightly to ~0.1 but remains relatively small. For comparison, a log plot of I_{dry} is plotted for comparison.

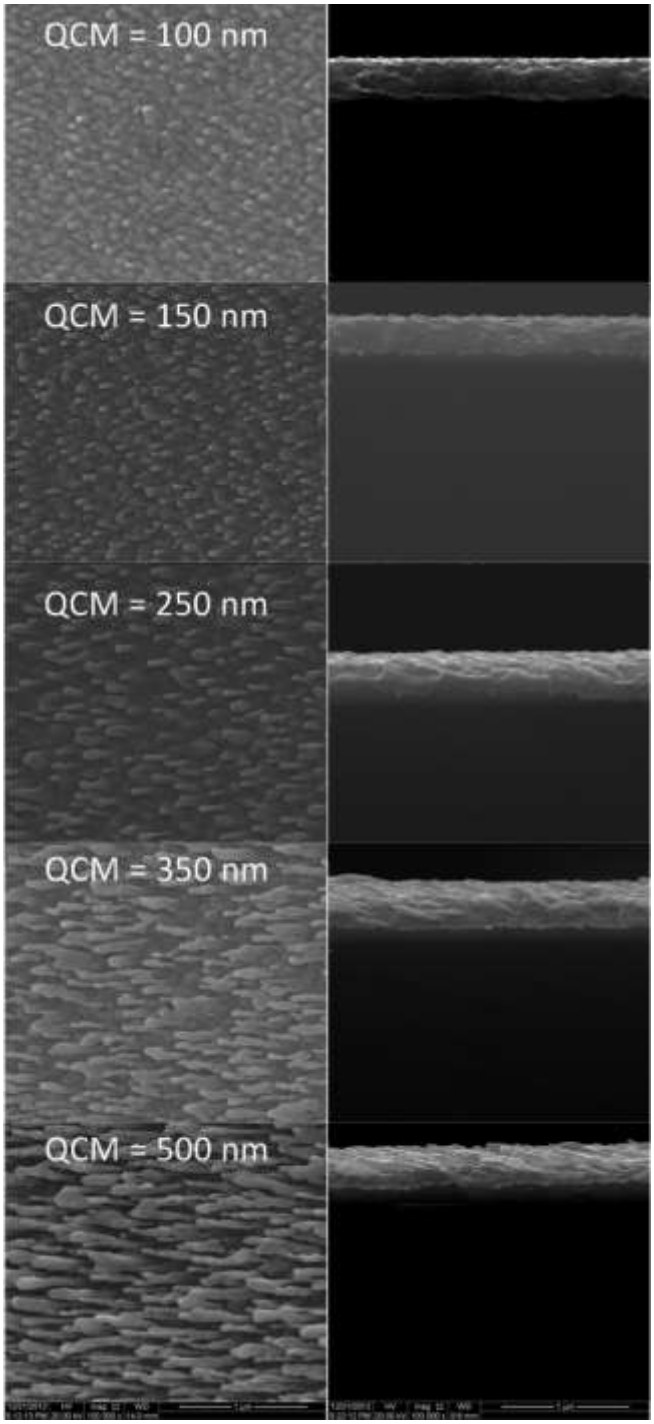

Figure S4. SEM analysis showing top view (left) and cross section (right) of AgNRs deposited onto underlying Ag film with varying QCM thicknesses. The magnification is 100,000× for all images.

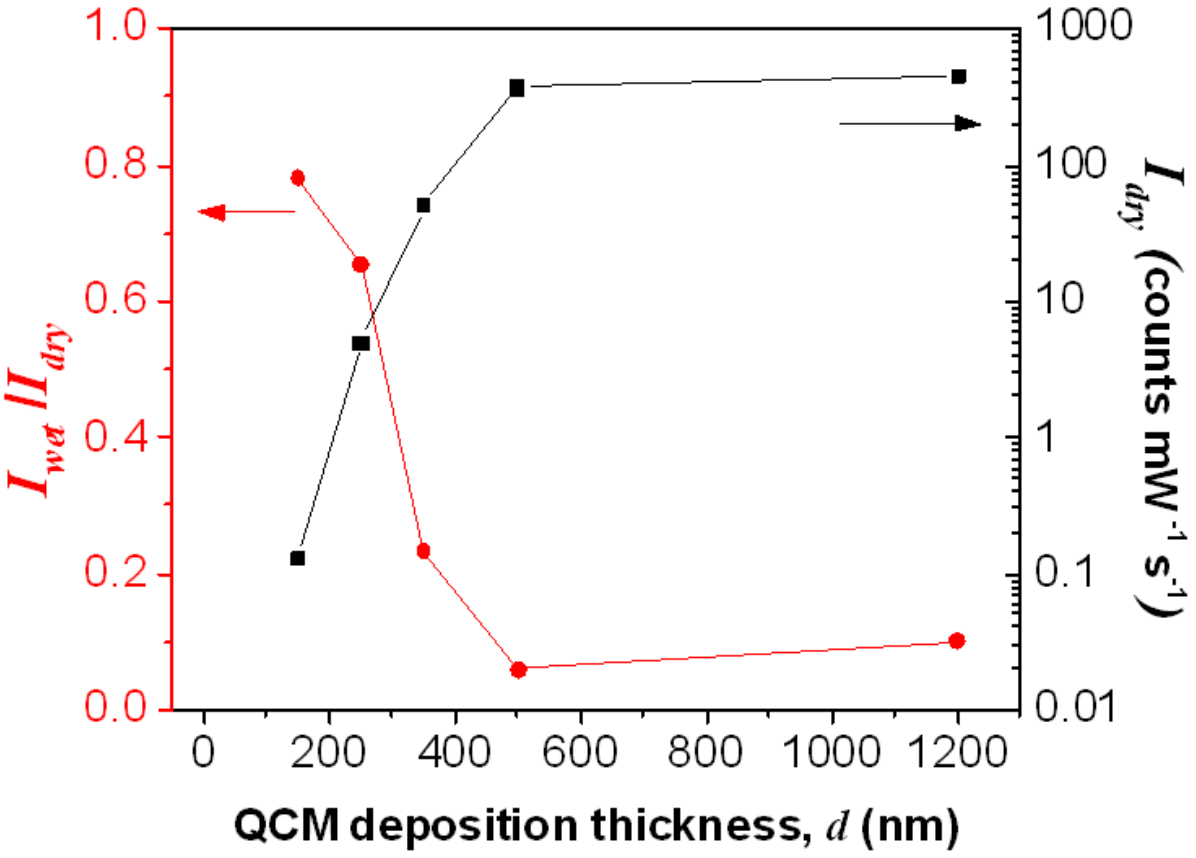

Figure S5. I_{wet}/I_{dry} ratio of MPh signal acquired on AgNR films (functionalized with a monolayer of MPh) as a function of AgNR length, represented by the QCM deposition thickness (red, scaled by left y-axis). A log plot of the corresponding I_{dry} used to calculate I_{wet}/I_{dry} is also shown for comparison (black, scaled by right y-axis).

S.6 Reversible Hot Spot Formation –Effect of Solvent Polarity on MH-Functionalized AgNRs

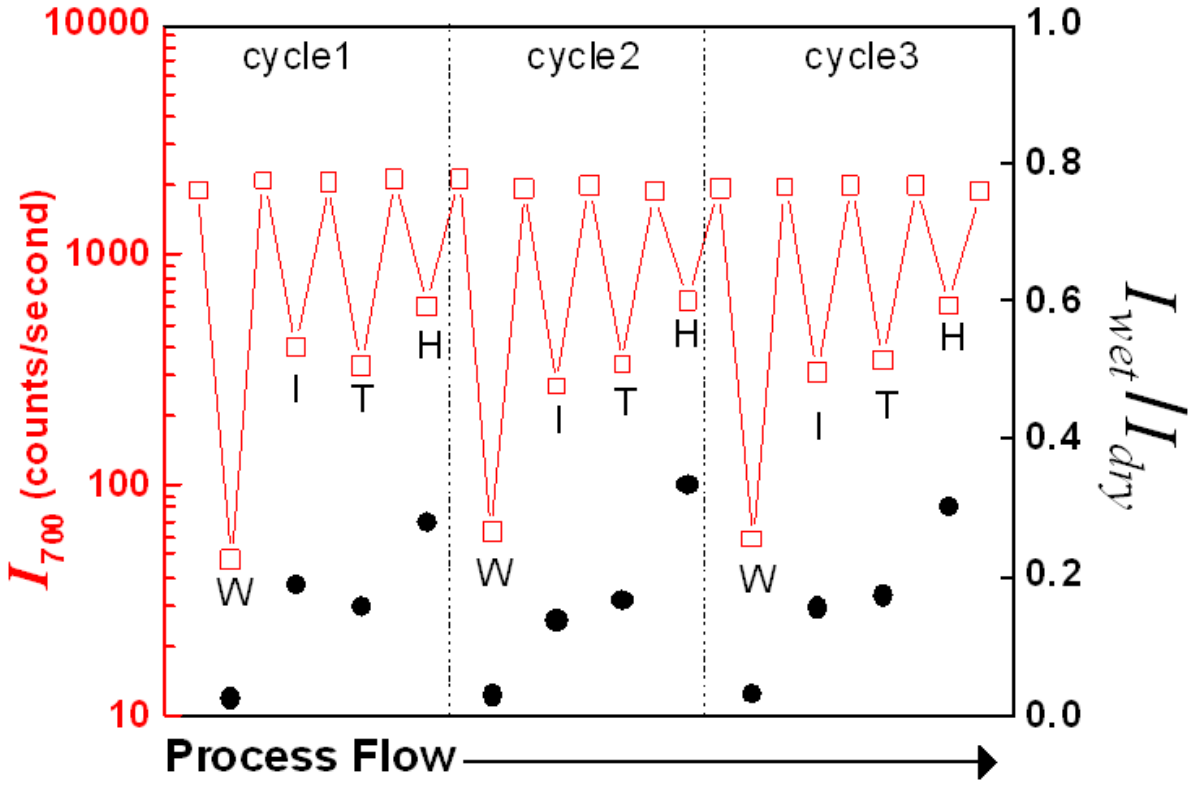

Figure S6. SERS intensity of 700 cm^{-1} peak measured on AgNR functionalized with a monolayer of MH. Measurements were acquired with the AgNRs in air (I_{dry}) or while immersed in solvent (I_{wet}) for three cycles. The x-axis represents the process flow of the processing/measurement conditions; W = water, I = IPA, T = toluene, and H=hexane; the values in between are the I_{dry} measurements. Three consecutive and identical cycles were performed. The red squares represent the I_{wet} and I_{dry} (plotted with respect to the log scale of the left y-axis). The black circles represent the I_{wet}/I_{dry} ratios for each liquid measurement and its preceding dry measurement (plotted with respect to the right y-axis).

With the exception of the IPA measurement in the first cycle, the results are very reproducible and consistent with the data in Figure 2.

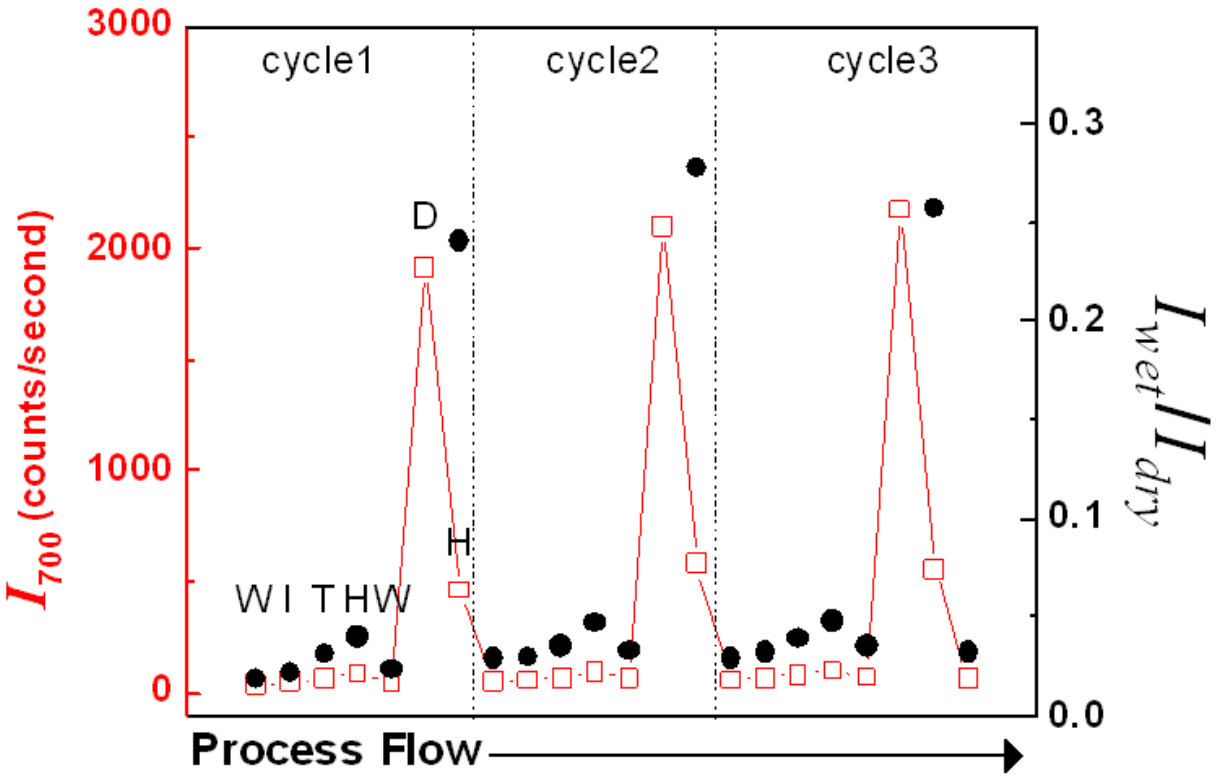

Figure S7. SERS intensity of 700 cm^{-1} peak measured on AgNR functionalized with a monolayer of MH. Measurements were acquired with the AgNRs air (I_{dry}) or while immersed in solvent (I_{wet}) for three cycles. The x-axis represents the process flow of the processing/measurement conditions; D = dry, W = water, I = IPA, T = toluene, and H=hexane. The red squares represent the I_{wet} and I_{dry} (plotted with respect to the log scale of the left y-axis). The black circles represent the I_{wet}/I_{dry} ratios for each liquid measurement and its preceding dry measurement (plotted with respect to the right y-axis).

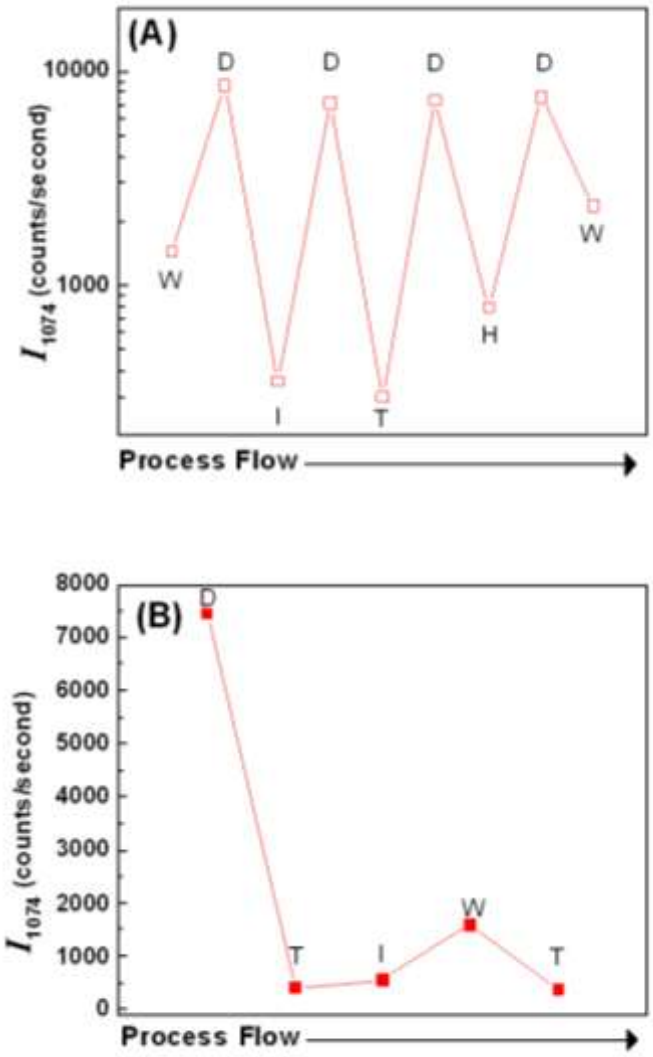

Figure S8. SERS intensity of the 1074 cm^{-1} peak of a benzenethiol monolayer on AgNR . These measurements are essentially the same as that shown in Figures S6 and S7, except that only one cycle is performed. The x-axis represents the process flow of the treatment conditions; D = dry, W = water, I = IPA, T = toluene, and H=hexane: A) drying after each solvent treatment, and B) changing solvents without drying (note that hexane was not used for in part B).

From Figure S8A we can see that the I_{1074} of hydrophobic benzenethiol decreases significantly when wet (~90%), even with water, but water produces a noticeably higher I_{wet} signal than toluene, IPA, and hexane, which is expected based on our solvent-induced de-bundling theory. For water on the hydrophobic AgNRs we would expect ~ 50% drop in intensity, similar to what we see with hexane treatment of dried hydrophilic-coated AgNRs. To understand this discrepancy, further investigations is warranted before a clear explanation can be proposed. From Figure S8B, we can see that water appears to cause some degree of bundling, even if the nanorods are not allowed to dry, which is similar to the small increase in I_{wet} observed for the hexane treatment (following the toluene treatment) in Figure S7.

References for Supporting Information

1. S. B. Chaney, S. Shanmukh, R. A. Dluhy and Y. P. Zhao, *Appl. Phys. Lett.*, 2005, **87**.
2. J. D. Driskell, S. Shanmukh, Y. Liu, S. B. Chaney, X. J. Tang, Y. P. Zhao and R. A. Dluhy, *J. Phys. Chem. C*, 2008, **112**, 895-901.
3. M. S. Schmidt, J. Hubner and A. Boisen, *Advanced Materials*, 2012, **24**, OP11-OP18.
4. H. B. Zhou, Z. P. Zhang, C. L. Jiang, G. J. Guan, K. Zhang, Q. S. Mei, R. Y. Liu and S. H. Wang, *Analytical Chemistry*, 2011, **83**, 6913-6917.
5. A. Kim, F. S. Ou, D. A. A. Ohlberg, M. Hu, R. S. Williams and Z. Y. Li, *Journal of the American Chemical Society*, 2011, **133**, 8234-8239.
6. J. G. Fan, J. X. Fu, A. Collins and Y. P. Zhao, *Nanotechnology*, 2008, **19**, 045713.
7. H. Liu, Y. Sun, Z. Jin, L. Yang and J. Liu, *Chemical Science*, 2013.
8. L. Yang, H. Liu, Y. Ma and J. Liu, *Analyst*, 2012, **137**, 1547-1549.